

Mechanistic Basis for Suicide Inactivation of Porphobilinogen Synthase by 4,7-Dioxosebacic Acid, an Inhibitor That Shows Dramatic Species Selectivity[†]

Jukka Kervinen,[‡] Eileen K. Jaffe,^{*‡} Frédéric Stauffer,[§] Reinhard Neier,[§] Alexander Wlodawer,^{||} and Alexander Zdanov^{||}

Institute for Cancer Research, Fox Chase Cancer Center, 7701 Burholme Avenue, Philadelphia, Pennsylvania 19111, Department of Chemistry, University of Neuchatel, Neuchatel 2007, Switzerland, and Macromolecular Structure Laboratory, National Cancer Institute, Frederick, Maryland 21702

Received April 2, 2001; Revised Manuscript Received May 15, 2001

ABSTRACT: 4,7-Dioxosebacic acid (4,7-DOSA) is an active site-directed irreversible inhibitor of porphobilinogen synthase (PBGS). PBGS catalyzes the first common step in the biosynthesis of the tetrapyrrole cofactors such as heme, vitamin B₁₂, and chlorophyll. 4,7-DOSA was designed as an analogue of a proposed reaction intermediate in the physiological PBGS-catalyzed condensation of two molecules of 5-aminolevulinic acid. As shown here, 4,7-DOSA exhibits time-dependent and dramatic species-specific inhibition of PBGS enzymes. IC₅₀ values vary from 1 μM to 2.4 mM for human, *Escherichia coli*, *Bradyrhizobium japonicum*, *Pseudomonas aeruginosa*, and pea enzymes. Those PBGS utilizing a catalytic Zn²⁺ are more sensitive to 4,7-DOSA than those that do not. Weak inhibition of a human mutant PBGS establishes that the inactivation by 4,7-DOSA requires formation of a Schiff base to a lysine that normally forms a Schiff base intermediate to one substrate molecule. A 1.9 Å resolution crystal structure of *E. coli* PBGS complexed with 4,7-DOSA (PDB code 1I8J) shows one dimer per asymmetric unit and reveals that the inhibitor forms two Schiff base linkages with each monomer, one to the normal Schiff base-forming Lys-246 and the other to a universally conserved “perturbing” Lys-194 (*E. coli* numbering). This is the first structure to show inhibitor binding at the second of two substrate-binding sites.

Porphobilinogen synthase (PBGS,¹ EC 4.2.1.24, also known as 5-aminolevulinic acid dehydratase) is a highly conserved metalloenzyme that functions in the first common step of the biosynthesis of the essential tetrapyrroles. The PBGS-catalyzed reaction is an asymmetric condensation between two molecules of 5-aminolevulinic acid (ALA) as described in Figure 1A. The crystal structure of the enzyme has been established for PBGS from yeast, *Escherichia coli*, and *Pseudomonas aeruginosa* (1–3). Some of the published structures contain the bound inhibitor levulinic acid, a complex analogous to the first enzyme-bound intermediate (2–4), which is a Schiff base formed between the keto group of P-side ALA (see Figure 1A) and the amino group of an invariant lysine residue (see Figure 2A). These structures delineated the locations of several different divalent metal ions and the binding residues for the carboxylic acid moieties

[†] This work was supported by Grant ES03654 (E.K.J.) from the National Institute of Environmental Health Sciences, NIH, by NIH Grant CA06927 (ICR), and by an appropriation from the Commonwealth of Pennsylvania. Its contents are solely the responsibility of the authors and do not necessarily represent the official views of the National Cancer Institute nor of the National Institute of Environmental Health Sciences.

* To whom correspondence and reprint requests should be addressed. Telephone: 215-728-3695. Fax: 215-728-2412. E-mail: EK_Jaffe@fccc.edu.

[‡] Fox Chase Cancer Center.

[§] University of Neuchatel.

^{||} National Cancer Institute.

¹ Abbreviations: PBGS, porphobilinogen synthase; ALA, 5-aminolevulinic acid; βME, 2-mercaptoethanol; BTP, 1,3-bis[tris(hydroxymethyl)methylamino]propane; 4,7-DOSA, 4,7-dioxosebacic acid.

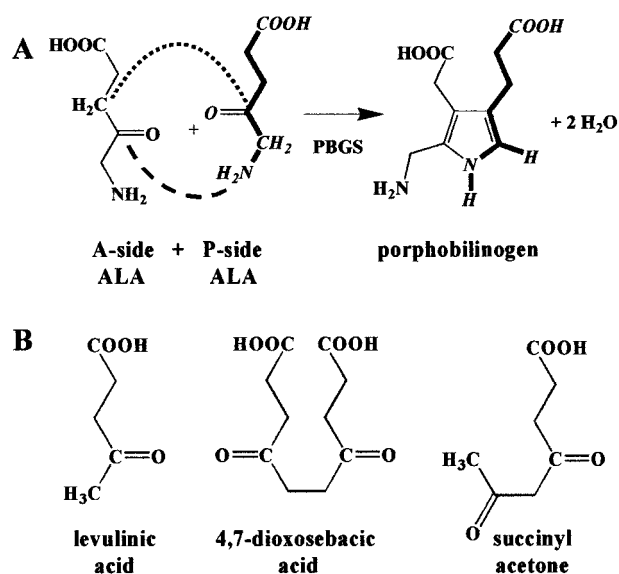


FIGURE 1: PBGS-catalyzed reaction and active site-directed inhibitors. (A) PBGS catalyzes the asymmetric condensation of two molecules of 5-aminolevulinic acid (ALA). A-side ALA (normal font) contributes the acetyl side chain and retains a free amino group. P-side ALA (bold bonds, italic font) contributes the propionyl side chain and has its amino group incorporated into the pyrrole ring. (B) PBGS inhibitors levulinic acid, 4,7-DOSA, and succinyl acetone.

of the two ALA substrate molecules. Despite the fact that PBGS is an octamer of ~300 kDa, the catalytic and binding residues at each active site derive from only one subunit.

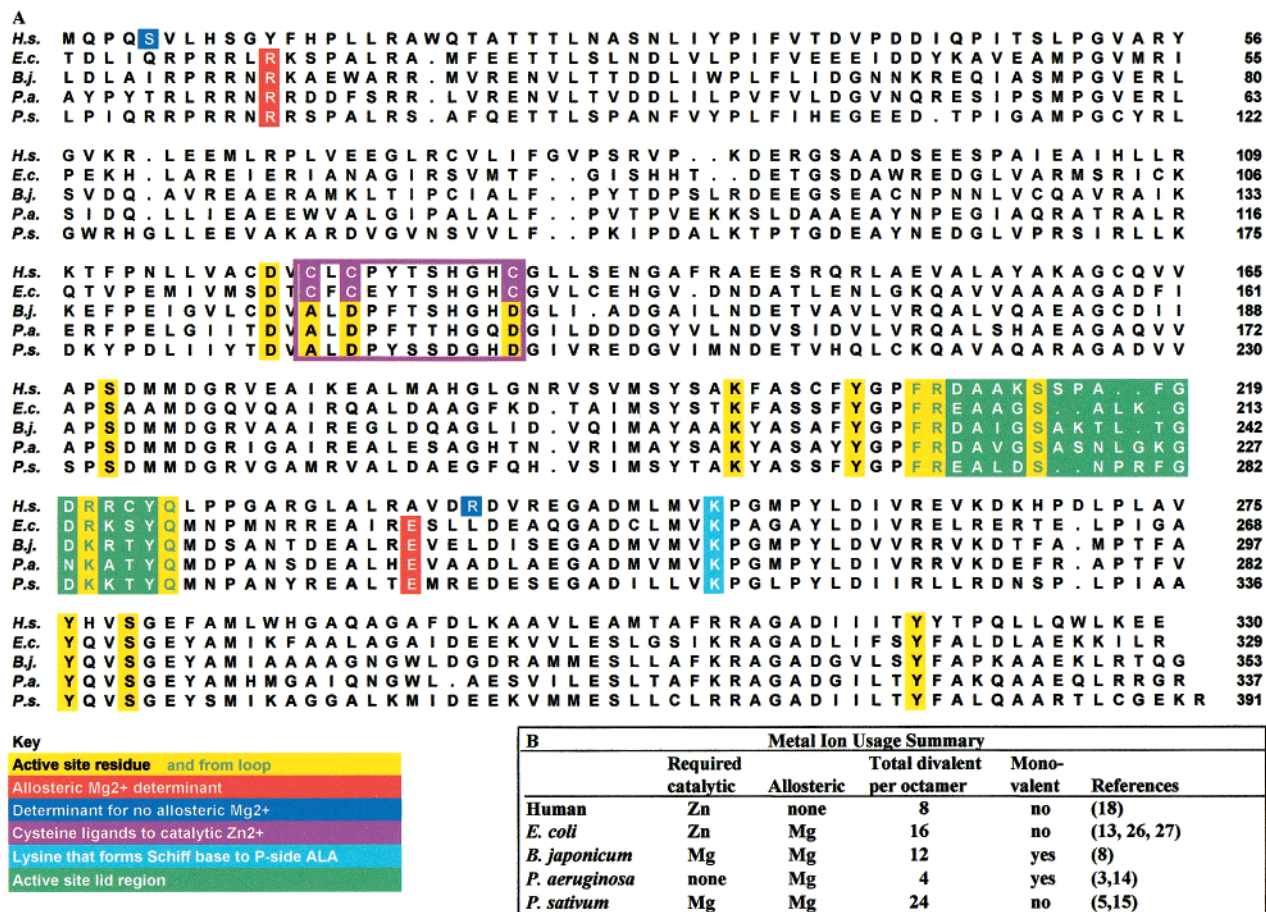


FIGURE 2: (A) Aligned sequences of PBGS from human (H.s.), *E. coli* (E.c.), *B. japonicum* (B.j.), *P. aeruginosa* (P.a.), and *P. sativum* L. (P.s.). Only the 330 amino acid core of the protein is illustrated. Additional N-terminal sequence information is omitted. All sequences are numbered starting at what is believed to be the normal physiological N-terminus (for B.j. and P.s., not known). Amino acids known to lie in the region of the enzyme active site are shown on yellow background. The residues on or in green approximate the location of the active site lid, the sequence of which is not highly conserved. The region boxed in purple depicts a unique metal binding site that contributes much of the active site diversity to the PBGS family of enzymes. It determines some of the metal ion requirements of these proteins. The cysteines that are ligands to an unusual catalytic Zn²⁺ are shown on purple; their presence or absence indicates whether a PBGS family member requires Zn²⁺ for activity. The red background shows the determinants for the allosteric Mg²⁺ which lies outside the active site and at subunit interfaces. The *E. coli* PBGS sequence is the only one shown that has both the catalytic Zn²⁺ and the allosteric Mg²⁺. The blue background shows the compensating arginine–serine pair for PBGS that lacks the allosteric Mg²⁺ (16). Other mammalian and yeast PBGS whose sequences are not shown have this arginine–serine pair. The lysine on cyan background is the P-side Schiff base-forming lysine. (B) Summary of the known metal ion usage of the five PBGS proteins for which the sequence is illustrated.

Nevertheless, there is some evidence suggesting that subunit interactions are essential to catalytic function (e.g., ref 5).

One truly unique feature of the PBGS family of enzymes is an apparent switch between the use of an active site Zn²⁺ and an active site Mg²⁺ (6, 7). Although the location of Mg²⁺ in place of the Zn²⁺ seen at the active site has yet to be established by crystallography, there is substantial kinetic support for Zn²⁺-free PBGS enzymes that absolutely require Mg²⁺ (5, 8). This apparent switch between Zn²⁺ and Mg²⁺ translates to a significant variation in the amino acids that occupy one area of the active site, as illustrated in Figure 2A. There may be mechanistic differences between those PBGS that have Zn²⁺ at the active site and those that do not. This difference in the active site structure and mechanism might translate into species-selective inhibition of tetrapyrrole biosynthesis, with the potential for commercial utility in agriculture and the pharmaceutical industry.

The structural details derived from the existing crystal structures do not unequivocally define the catalytic mechanism, the roles of the metal ions, or the mechanistically

significant subunit interactions. Notably absent from the crystal structures is information on the accepting groups for the four protons that are formally lost as water in the reaction illustrated in Figure 1A. Another uncertainty is the order of bond formation between the two ALA substrate molecules. It is not known if carbon–carbon bond formation (aldol condensation) precedes or follows the intersubstrate carbon–nitrogen bond formation. To address the latter question, a series of potential bisubstrate and intermediate analogues have been characterized with PBGS (9–11). The analogues mimic structures that might be present in each of the two mechanisms. The most recent results with *E. coli* PBGS have been interpreted as supporting a mechanism in which carbon–nitrogen bond formation precedes carbon–carbon bond formation (11).

The current work expands on studies of the most potent inhibitor, the diketo compound 4,7-dioxosebacic acid (4,7-DOSA, illustrated in Figure 1B), which was found to act as an irreversible inhibitor of *E. coli* PBGS (11). Because we have engaged in the systematic characterization of PBGS

from a variety of species, we have investigated whether 4,7-DOSA shows any selectivity in its potency with PBGS from different species. The species investigated are human (12), *E. coli* (13), *Bradyrhizobium japonicum* (7, 8), *P. aeruginosa* (14), and *Pisum sativum* (garden pea) (5, 15). The sequences of these five enzymes are illustrated in Figure 2A. Figure 2B summarizes what is known of the divalent and monovalent metal ion utilization by these enzymes (see also ref 16). Investigations of the inhibitor with human PBGS is extended here to include variants with specific mutations to active site residues (17, 18). The structural basis for inhibition of *E. coli* PBGS by 4,7-DOSA has been determined by X-ray crystallography. The resulting 1.9 Å resolution structure of the covalent enzyme–inhibitor complex formed in the inactivation reaction reveals cross-linking to a second reactive lysine and suggests a mechanistic basis for the physiologically significant inactivation of PBGS by succinyl acetone (4,6-dioxoheptanoic acid), a related inhibitor that occurs during tyrosinemia.

MATERIALS AND METHODS

Materials. Most chemicals and buffers were obtained from Fisher Scientific (Pittsburgh, PA) or Sigma-Aldrich (St. Louis, MO) in the purest available form. 2-Mercaptoethanol (β ME) from Fluka (Buchs, Switzerland) was vacuum-distilled prior to use. 4,7-Dioxosebacic acid (4,7-DOSA) was synthesized and tested as described in ref 11. All of the PBGS enzymes used in this study were cloned and expressed in *E. coli*, and their purification and detailed characterization have been described earlier (5, 8, 12–14, 19). There are two common kinetically comparable human PBGS alleles, N59 and K59 (12, 20). Human PBGS was the C162A variant of the natural N59 isozyme and has kinetic properties closely resembling those of the wild type (18). The human PBGS mutants characterized were N59/C162A/H131A/C223A (called MinusZnA) (18) and K59/K252G (called K252G) (17).

Activity Assays for PBGS. The routine enzyme assay was used which measures the formation of porphobilinogen from ALA. The optimal assay conditions for human PBGS were 0.1 M potassium phosphate, pH 7.0, 10 mM β ME, and 10 μ M ZnCl₂; for *E. coli* PBGS, 0.1 M 1,3-bis[tris(hydroxymethyl)methylamino]propane hydrochloride (bis-tris) (BTP-HCl), pH 8.1, 10 mM β ME, 10 μ M ZnCl₂, and 1 mM MgCl₂; for *B. japonicum* PBGS, 0.1 M BTP-HCl, pH 8.5, 10 mM β ME, and 10 mM MgCl₂; for *P. aeruginosa* PBGS, 0.1 M BTP-HCl, pH 8.5, and 10 mM MgCl₂; and for *P. sativum* PBGS, 0.1 M BTP-HCl, pH 8.5, 10 mM β ME, and 10 mM MgCl₂. Each PBGS was preincubated in its optimal assay solution (35 μ g mL⁻¹, corresponding to \sim 1 μ M subunit) for 10 min at 37 °C prior to the addition of the substrate ALA-HCl to a final concentration of 10 mM, which lowers the assay solution pH about 0.2 unit. The reaction was allowed to proceed for 5 min prior to termination with a one-half volume of STOP reagent (20% trichloroacetic acid, 0.1 M HgCl₂). For *P. aeruginosa* PBGS the STOP reagent did not contain HgCl₂. Precipitated protein and β ME were removed by centrifugation. The quenched assay solutions were diluted 1:3–25 with a 2:1 mixture of assay buffer and STOP reagent, and then 0.5 mL of diluted solutions was mixed with 0.5 mL of modified Ehrlich's reagent. Color development was allowed to proceed for about 8 min, and the porphobilinogen formed was determined by absorbance at 555 nm ($\epsilon_{555} =$

62 000 M⁻¹). Specific activity is defined as micromoles of porphobilinogen formed per hour per milligram of protein. Human mutant MinusZnA was assayed in the same fashion as the wild type. For human mutant K252G the assay time was extended up to 41 h. Enzyme concentrations were measured with Coomassie Plus protein assay reagent (Pierce, Rockford, IL) relative to a standard curve prepared with bovine serum albumin.

Inhibition of PBGS by 4,7-DOSA. The five species of PBGS (1 μ M subunit) were preincubated under their optimal assay conditions for 10 min at 37 °C prior to the addition of 4,7-DOSA over the concentration range of 0.2 μ M–2 mM; the preincubation was allowed to proceed for an additional 100 min at 37 °C before the formation of porphobilinogen was initiated by addition of ALA to a final concentration of 10 mM. For human PBGS (0.2 μ M subunit), preincubation times of 10 min, 30 min, 100 min, and 16 h with 4,7-DOSA were evaluated over the full range of [4,7-DOSA]. For pea PBGS (1 μ M subunit), preincubation times of 10 min, 30 min, 100 min, 5 h, and 30 h were evaluated using 2 mM 4,7-DOSA. Most data were fitted to standard or cited equations using the program SigmaPlot (SPSS Inc., Chicago, IL).

Crystallization of *E. coli* PBGS Complexed with 4,7-DOSA and Structure Solution. *E. coli* PBGS (9 mg/mL in 50 mM Tris-HCl, pH 8.0, 10 mM β ME, 20 μ M ZnCl₂, 10 mM MgCl₂) was incubated with a 16-fold molar excess of 4,7-DOSA (stock: 40 mM in 0.1 M Tris-HCl, pH 7.5) for 16 h. Crystallizations were carried out using the sitting-drop vapor diffusion technique at room temperature by mixing the clarified protein solution with an equal volume of the reservoir buffer containing 2.5% poly(ethylene glycol) 3350 (Sigma), 10% glycerol, 0.1 M Tris-HCl, pH 8.5, and 0.02% sodium azide. The crystals with a diamond-like shape appeared in 1–3 days and grew to their final size in about 2 weeks. Cryoprotection was carried out by transferring a crystal to reservoir solutions containing 17%, 23%, and 30% glycerol, respectively (3 min in each solution), and the crystal was flash-frozen in a liquid nitrogen vapor. X-ray diffraction data were collected from one crystal (0.4 \times 0.4 \times 0.2 mm) at 100 K using a MAR345 image plate mounted on a Rigaku RU-200 rotating anode generator equipped with OSMIC mirror optics, operated at 50 kV and 100 mA. The data set consisted of 132 frames corresponding to 1.0° oscillation exposed for 7 min each. Crystals belong to a tetragonal system, space group *P*4₂1₂, unit cell parameters $a = b = 128.7$ Å and $c = 142.8$ Å, and there are two subunit molecules per asymmetric unit. Diffraction intensities were processed with the HKL2000 suite of programs (21), $R_{\text{merge}}(I) = 6.9\%$ for 94 536 independent reflections, with completeness of 99.9% for the 35–1.9 Å resolution range.

The structure was solved by molecular replacement with the AmoRe program package (22), using *E. coli* PBGS structure coordinates 1b4e (2) as an initial model. Refinement was carried out with program package CNS (23) with very weak noncrystallographic symmetry (NCS) restraints. At the beginning of the refinement the NCS restraint weight was 100; at the end it was 25. Model building was done with the program O (24). The final model included one dimer of PBGS molecules complexed with two inhibitor molecules, 312 water molecules, two Zn²⁺ ions, and two Mg²⁺ ions. The crystallographic *R*-factor is 19.8% and *R*(free) is 24.9%

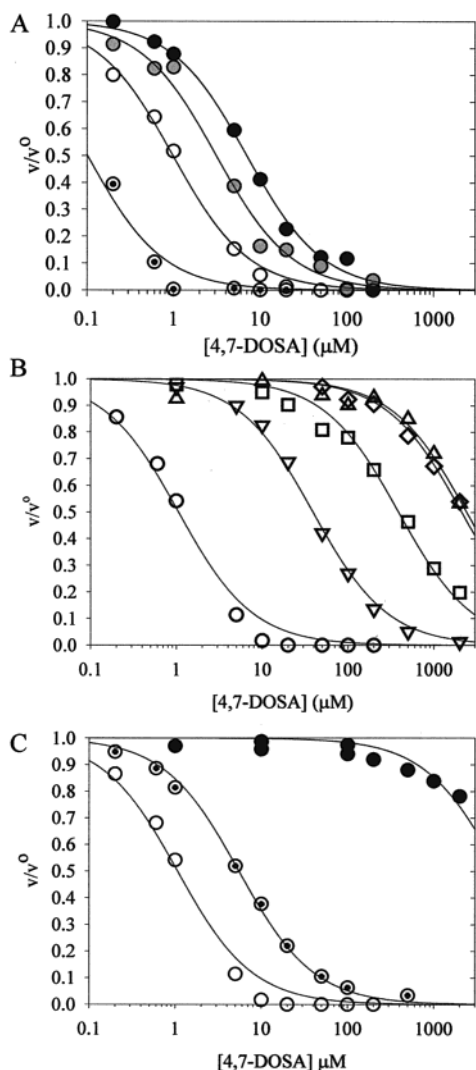


FIGURE 3: Dose–response curves for various PBGS with 4,7-DOSA. Lines are the best fits to eq 1 in the text. (A) Inactivation of human PBGS by 4,7-DOSA. The inhibitor–enzyme incubation time (prior to addition of substrate) is 10 min (●), 30 min (gray circle), 100 min (○), and 16 h (◐). For these curves, the enzyme subunit concentration was 0.2 μM . (B) Inactivation of a family of PBGS enzymes by 4,7-DOSA using a fixed 100 min inhibitor–enzyme incubation time. The species are human (○), *E. coli* (▽), *B. japonicum* (□), *P. aeruginosa* (◇), and pea (△). For these determinations, the protein concentrations were all at 1 μM subunit. (C) Inactivation of human PBGS variants using a 100 min incubation time. The wild-type variant N59/C162A is (○), MinusZnA (N59/C162A,H131A,C223A) is (◐), and the active site lysine mutant (K252G) is (●). The line used to illustrate the K252G data is not a fit.

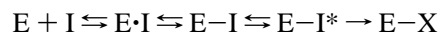
for 1.9 Å resolution data, and the RMS deviations for bond lengths and bond angles are 0.018 Å and 1.9°, respectively. The coordinates have been deposited in the Protein Data Bank with the PDB code 1I8J for immediate release.

RESULTS

Kinetic Evaluation of the Inhibition of Wild-Type Human PBGS by 4,7-DOSA. The inactivation of PBGS by 4,7-DOSA is dependent upon both the concentration of the inhibitor and the preincubation time of the inhibitor and enzyme prior to addition of substrate. Figure 3A illustrates this relationship for the interaction of 4,7-DOSA with human PBGS using a fixed enzyme subunit concentration of 0.2 μM , enzyme–

inhibitor incubation times of 10 min, 30 min, 100 min, and 16 h, and inhibitor concentrations from 0.2 to 200 μM . The data indicate that the inactivation of human PBGS by 4,7-DOSA is a function of time, is relatively slow, and at long times is impressively potent. For instance, when 0.2 μM 4,7-DOSA and 0.2 μM human PBGS subunits are incubated for 16 h, there is greater than 50% inhibition. The control reactions wherein inhibitor was omitted did not lose any significant activity.

A quantitative analysis of the inactivation data is shown as best fit lines in Figure 3. 4,7-DOSA is a symmetric molecule that mimics C1 to C5 of each ALA substrate molecule but lacks the C5 amino moieties (see Figure 1). The interaction of 4,7-DOSA with PBGS (I and E, respectively, in the scheme below) is presumed to proceed in a manner analogous to the interaction of ALA with PBGS. The first interaction is expected to be one-half of the inhibitor, C1 to C5, binding to the P-side ALA binding pocket to form the E·I complex and the subsequent formation of a Schiff base linkage between C4 and Lys-246, which is the E–I complex. These two steps should be rapid and reversible. At some point there is binding of C6 to C10 of 4,7-DOSA to the A-side ALA binding pocket. Since the carboxyl group of A-side ALA has been proposed to interact with arginines that derive from an active site lid (3), one might propose that this form of the enzyme–inhibitor complex (E–I*) is less freely reversible than E–I. Finally, since we see an irreversible inhibition, the assumption is that additionally covalent interactions occur to form E–X and the overall process of enzyme inactivation is complete. The equation for the overall reaction can be written as



Although this reaction is complex and more than one alternate order of kinetic steps is possible, dissection of the kinetic interactions of 4,7-DOSA with PBGS is not expected to yield significant new information applicable to understanding the normal PBGS-catalyzed reaction. Hence, for the purpose of analyzing the inhibition data, the approximation of a tight binding inhibitor is used according to the method of Copeland for estimating IC_{50} values (25). This approximation is consistent with the prior classification of 4,7-DOSA as a slow tight binding inhibitor of *E. coli* PBGS (11). The inactivation data at each incubation time are fitted to the equation:

$$v/v^0 = 1/[1 + ([I]/\text{IC}_{50})] \quad (1)$$

where v/v^0 is the fractional activity of the inhibited enzyme and [I] is the concentration of 4,7-DOSA. The apparent IC_{50} values corresponding to 10 min, 30 min, 100 min, and 16 h for human PBGS are 7.0 ± 0.4 , 2.8 ± 0.2 , 0.98 ± 0.06 , and 0.10 ± 0.01 μM , respectively. The data presented in Figure 3A show 4,7-DOSA to be a much more potent inactivator of human PBGS than was previously reported for the inhibitor with *E. coli* PBGS (11). Hence, we evaluated each of the PBGS on hand to determine whether there is a species selectivity to the potency of 4,7-DOSA against PBGS.

Inactivation of Various PBGS by 4,7-DOSA. The ability of 4,7-DOSA to inhibit PBGS from human, *E. coli*, *B. japonicum*, *P. aeruginosa*, and pea was determined as illustrated in Figure 3B. The assays used an enzyme–

inhibitor incubation time of 100 min and an enzyme subunit concentration of 1 μM . The enzyme concentration was dictated by a propensity of some (but not all) PBGS to dissociate into less active multimers at protein concentrations below 1 μM (5, 8, 14). A comparison of the 100 min data (open circles in panels A and B of Figure 3) illustrates that little changes when the human PBGS concentration is changed from 0.2 to 1 μM ; in both cases the apparent IC_{50} is $\sim 1 \mu\text{M}$. These dose–response curves were carried out at the optimal activity conditions for each of the PBGS studied.

The data illustrated in Figure 3B show a remarkable species selectivity to the 4,7-DOSA inactivation phenomenon. The lines are nonlinear best fits to eq 1 (above), and the respective IC_{50} values for human, *E. coli*, *B. japonicum*, *P. aeruginosa*, and pea PBGS are calculated to be 1.1 ± 0.1 , 39 ± 2 , 390 ± 30 , 2100 ± 100 , and $2400 \pm 700 \mu\text{M}$, respectively, showing a dramatic 2000-fold variation in potency under these conditions. The IC_{50} values are not related to the inherent specific activities of the PBGS from these same species, which for the uninhibited samples used herein are respectively 36, 69, 24, 52, and 235 $\mu\text{mol h}^{-1} \text{mg}^{-1}$. The IC_{50} values also do not reflect any inherent differences in the K_m values for ALA, which under these assay conditions all lie in the range of $100 \pm 50 \mu\text{M}$. In general, the Zn^{2+} -dependent PBGS are found to be far more susceptible to inactivation by 4,7-DOSA than those PBGS that do not require Zn^{2+} (see Figures 2B and 3B).

4,7-DOSA is such a poor inhibitor of pea PBGS that we considered whether the inhibition might not be simply competitive and reversible. Hence, pea PBGS (1 μM monomer) was mixed with 2 mM 4,7-DOSA, and the activities were evaluated after 10 min, 30 min, 100 min, 5 h, and 30 h preincubation times. The resultant activities were 71%, 63%, 54%, 50%, and 34%, respectively, compared to activities obtained without the inhibitor. We conclude that although 4,7-DOSA is a very poor inhibitor for pea PBGS, the inhibition still occurs in a time-dependent manner and suggests that the inhibitor slowly forms an irreversible complex with the enzyme.

Evaluation of 4,7-DOSA with Active Site Mutant Forms of Human PBGS. The interaction of 4,7-DOSA with PBGS is presumed to rely partially upon the formation of a Schiff base between C4 of 4,7-DOSA and the active site lysine that normally interacts with C4 of P-side ALA. We thus examined inhibition of a site-directed mutant of human PBGS, K252G, which lacks this lysine moiety. Figure 3C illustrates the interaction of human PBGS variant K252G with 4,7-DOSA and shows that the mutant is dramatically less susceptible to inactivation (>6000 -fold). Thus, we conclude that the inactivation of human PBGS relies on the formation of the Schiff base intermediate with Lys-252 as presumed in the scheme above. However, since all of the native PBGS have a comparable lysine, interaction with the P-side Schiff base-forming lysine does not explain the high sensitivity of human PBGS for inactivation by 4,7-DOSA.

The data discussed above suggest that the catalytic Zn^{2+} is one determinant for high sensitivity to 4,7-DOSA. Although both human and *E. coli* PBGS require Zn^{2+} , human PBGS has two kinds of Zn^{2+} at the active site (18) while the *E. coli* PBGS crystal structure (PDB code 1b4e) shows only one at the active site. To evaluate whether this difference contributes to the differential sensitivity of human and *E.*

coli PBGS to 4,7-DOSA, we also investigated a second human PBGS site-directed mutant, a Zn^{2+} -binding mutant known as MinusZnA (18). MinusZnA is a catalytically active mutant that does not contain the Zn^{2+} that is absent in *E. coli* PBGS but does contain the Zn^{2+} that is present in *E. coli* PBGS. As illustrated in Figure 3C, MinusZnA is approximately 5-fold less susceptible than wild-type human PBGS to 4,7-DOSA inactivation. Thus, the existence and coordination of both types of Zn^{2+} in the human PBGS active site are seen to influence the binding or reactivity of 4,7-DOSA to the enzyme.

***E. coli* PBGS Crystal Structure with 4,7-DOSA.** The 1.9 Å crystal structure of *E. coli* PBGS that has been inactivated by 4,7-DOSA was solved and is shown in Figure 4. A major contribution of this structure is to show the likely position of enzyme-bound A-side ALA. Unlike the complex of *E. coli* PBGS with levulinic acid (PDB code 1b4e), there is a PBGS dimer, rather than a monomer, in the asymmetric unit formed by a noncrystallographic 2-fold axis (Figure 4A). Four such dimers make up the PBGS octamer (Figure 4B) around a crystallographic 4-fold symmetry axis. Both monomers of the dimer show that complex formation has occurred with 4,7-DOSA and that each monomer contains two divalent metal ions at 100% occupancy. The RMS deviation between the C α atoms of the two monomers of the dimer is 0.15 Å, whereas the RMS deviation between each monomer and the 1b4e structure is 0.32 and 0.34 Å, respectively. Thus there are no significant differences between the monomers of the dimer, although the conformations of some side chains, mainly those located on the surface of the octamer, are sometimes different. The conformation of the side chains and of inhibitor molecules in the active site is exactly the same in both crystallographically independent molecules. The average temperature factor is 31.4 Å² for monomer A and 32.2 Å² for monomer B, indicating that both molecules have essentially the same degree of flexibility. Therefore, even though there is a dimer of PBGS in the asymmetric unit in the crystal form containing 4,7-DOSA, both monomers are very much alike. This makes the structure of the current dimer very similar to that of 1b4e, where a dimer is made by a purely crystallographic 2-fold axis (space group I422).

The dimer reported here is remarkably different from the one found in the structure of the asymmetric dimer of *P. aeruginosa* PBGS (PDB code 1b4k) (3). In that case, monomer B was found in an “inactive state” without any metal ions bound, whereas monomer A was found in an “active state” containing Mg^{2+} at an allosteric site somewhat distant from the active site. In addition, monomer B had an average temperature factor about 5 Å² larger than that of monomer A. The most significant difference between monomers A and B was an important structural element, a lid covering the active site cleft, which was disordered in monomer B and ordered in monomer A. The buried surface area between monomers comprising the dimer in the present structure is almost the same, 3067 versus 2900 Å² in 1b4k, suggesting that the number of contacts between the monomers keeping them together is almost equal. However, the surface areas of the monomers themselves are not the same, being 14 726 and 15 388 Å² in 1b4k and 14 517 and 14 372 Å² in the current structure, suggesting that in the latter case both monomers, and particularly the second one, have a more

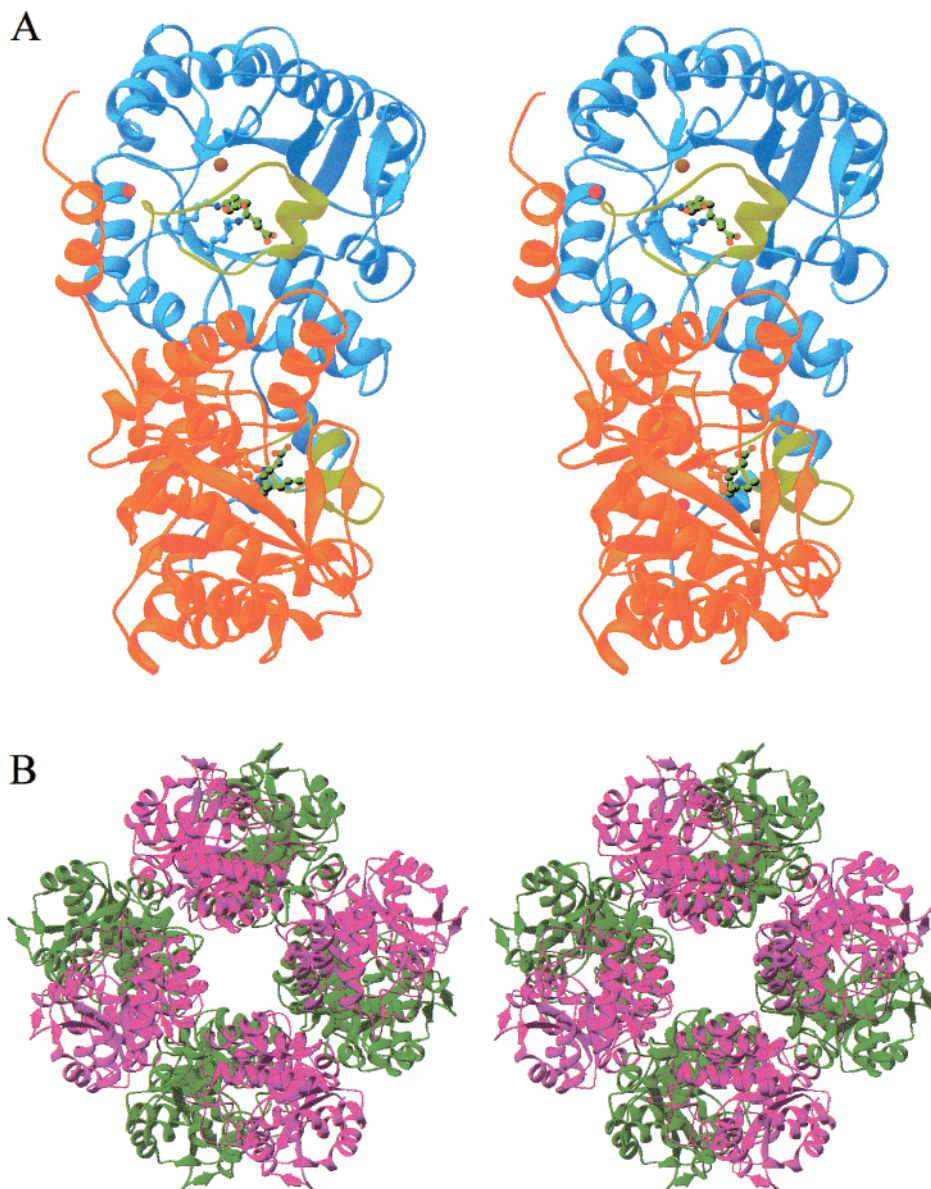


FIGURE 4: (A) Stereo diagram of the 4,7-DOSA-inactivated *E. coli* PBGS dimer. The two monomers are shown in blue and red, Zn^{2+} is in brown, Mg^{2+} is in orange, and the active site lid is in light green. The two active site lysine residues are shown as ball-and-stick models, and the carbon atoms are colored according to the subunit; ϵ -amino is in dark blue. The atoms derived from 4,7-DOSA are shown in ball-and-stick models with carbon atoms in green and the oxygen atoms in red. (B) Stereo diagram of the PBGS octamer where all subunits A are in magenta and all subunits B are in dark green.

compact fold. As a result, the whole dimer in the current structure is more compact with a surface area of 22 753 versus 24 447 \AA^2 in the 1b4k structure. Superposition of our dimer with that of 1b4k gives an RMS deviation of 1.13 \AA , while superposition of each of the respective monomers gives an RMS deviation of 0.97 \AA for monomer A and 1.20 \AA for monomer B. Taken together, we can conclude that, unlike the 1b4k dimer, our dimer consists of two “active” monomers. The ordered active site lid on both subunits is shown in light green in Figure 4A. The current structure does not explain the structural basis of some half-sites reactivity phenomena, like saturation at four enzyme-bound porphobilinogen, that have been documented biochemically for *E. coli* PBGS (e.g., ref 17).

Mechanism of Inhibition by 4,7-DOSA. The inhibitor molecule was clearly seen in the difference electron density map in the area of the active site next to Lys-194 and Lys-

246 in both monomers. Figure 5A illustrates an electron density map of the inhibitor bound to the enzyme. Each inhibitor molecule forms two covalent linkages to the protein as illustrated schematically in Figure 6. C1 through C5 of the inhibitor are bound in a manner analogous to the inhibitor levulinic acid contained in *E. coli* PBGS structure 1b4e with a Schiff base linkage between C4 and the ϵ -amino group of Lys-246. The comparison is shown in Figure 5B. The C1 carboxyl oxygens of the inhibitor make hydrogen bonds with Ser-272 and Tyr-311. These residues are conserved among PBGS enzymes and have previously been identified as the molecular determinants for the carboxyl group of P-side ALA (2, 3), which forms a Schiff base with Lys-246. The bond between C5 and C6 of the inhibitor has a distorted cis configuration (torsion angle C4–C5–C6–C7 is $\sim 65^\circ$) in order to accommodate the second Schiff base linkage between C7 and the ϵ -amino group of Lys-194. The Schiff

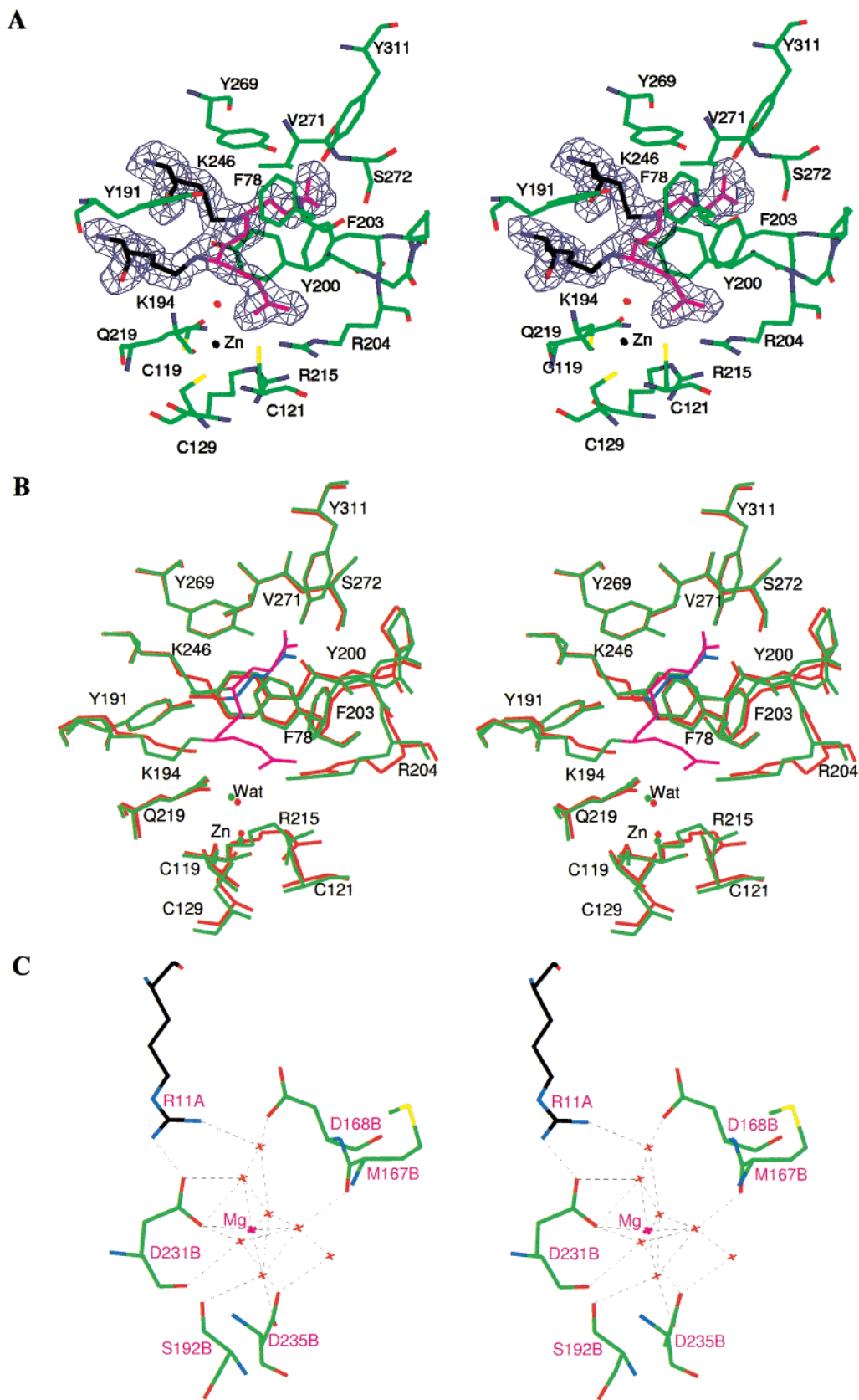


FIGURE 5: (A) Stereo picture of the electron density of the region around the inhibitor, Lys-194, Lys-246, and other active site components. The carbon atoms derived from 4,7-DOSA are in magenta. Carbons from Lys-194 and Lys-246 are in black. Carbons from protein are in green, nitrogen is in blue, oxygen is in red, sulfur is in yellow, and Zn^{2+} is in black. The illustration shows a $2F_o - F_c$ difference electron density map contoured at a level of 2σ . (B) Stereo overlay of 4,7-DOSA (magenta) inhibited *E. coli* PBGS (green) with levulinic acid (blue) inhibited *E. coli* PBGS (red). (C) Stereo diagram of the coordination of Mg^{2+} in the allosteric binding site. Water molecules are shown as red crosses, carbons from the A subunit are in black, and carbons from the B subunit are in green.

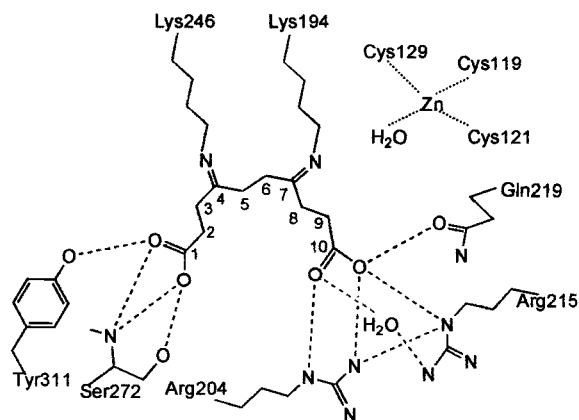


FIGURE 6: Schematic diagram of the 4,7-DOSA interaction with *E. coli* PBGS. The carbon atoms of 4,7-DOSA are numbered. Dashed lines indicate hydrogen bonds using a heteroatom distance of ≤ 3.1 Å as indicating a hydrogen bond. The dotted lines indicate the Zn^{2+} ligand bonds, which are each ~ 2.4 Å.

base to Lys-194 is believed to mimic the Schiff base that normally forms between C4 of A-side ALA and the C5 amino group of the P-side Schiff base and corresponds to the intermolecular carbon–nitrogen bond illustrated in Figure 1A. However, observation of this Schiff base linkage raises the possibility that A-side ALA might normally form a bond to Lys-194. The structure of 4,7-DOSA-inactivated *E. coli* PBGS is the first example of the reactivity of Lys-194, which is required to be uncharged for the Schiff base linkage to form. The remainder of the A-side ALA half of the inhibitor, C8 to C10, extends out toward the lid. The C10 carboxyl oxygens make hydrogen bond linkages with three residues (Arg-204, Arg-215, and Gln-219) in a continuous region of sequence (Figures 2A and 4A), portions of which are disordered in some PBGS crystal structures and thus considered a mobile active site lid (residues 196–219). Several ordered water molecules are within 5 Å of C8–C10.

Also illustrated in Figures 5A,B and 6 is the catalytically essential Zn^{2+} , an active site component that is shared by human and *E. coli* PBGS but absent from those PBGS much less sensitive to inhibition by 4,7-DOSA. The three amino acid ligands to this Zn^{2+} are cysteine residues that derive from a metal-binding region of the sequence that is boxed in Figure 2A. The sulfur atoms of Cys-119, Cys-121, and Cys-129 are each 2.4 Å from the Zn^{2+} and are arranged at three corners of a tetrahedron. The fourth coordination partner of the Zn^{2+} is a water molecule. This water ligand is 2.1 and 2.3 Å from the Zn^{2+} in the two subunits and respectively 3.6 and 4.0 Å from the C7 of 4,7-DOSA. The angles (Zn, O, C7) are both 122° . Thus, it appears that the Zn^{2+} -bound water molecule most likely derives from C7 of 4,7-DOSA. Hence, the Zn^{2+} is positioned to polarize the C7 carbonyl of 4,7-DOSA, thus assisting in formation of the Schiff base between C7 and the ϵ -amino group of Lys-194. For the normal PBGS-catalyzed reaction, the Zn^{2+} would be positioned to polarize the C4 carbonyl of A-side ALA, thus assisting in formation of a Schiff base that could form to Lys-194 or to the C5 amino group of P-side ALA. This mechanistic uncertainty is discussed below. In either case, the Zn^{2+} is proposed to be a significant determinant in the high sensitivity of the Zn^{2+} -requiring PBGS to inactivation by 4,7-DOSA.

Metal Ions of *E. coli* PBGS. *E. coli* PBGS binds a total of 16 divalent metal ions which can be either 16 Zn^{2+} or 8 Zn^{2+} plus 8 Mg^{2+} (26). In the latter configuration the enzyme experiences an allosteric activation. Relative to the 16 Zn^{2+} form of the enzyme, the Mg^{2+} -activated enzyme has a 2-fold increase in V_{max} , a 10-fold decrease in the K_m for ALA, and an increased affinity for the catalytically essential Zn^{2+} (27). The allosteric Mg^{2+} , which has been called MgC, was first seen bound to one-half the subunits of the *P. aeruginosa* PBGS structure 1b4k (3). It is located at the interface of the $\alpha\beta$ -barrel of one subunit and the arm of an adjacent subunit (see Figure 4A). The molecular details of the MgC site in the current structure are shown in Figure 5C. In the all- Zn^{2+} *E. coli* PBGS structure 1b4e, Zn^{2+} is seen at the MgC site. The location and extensive hydrogen-bonding network around MgC explain its previously demonstrated role in maintaining the quaternary structure of *E. coli* PBGS (27). Despite the kinetic differences between the 8 Zn^{2+} plus 8 Mg^{2+} form of the *E. coli* enzyme presented here and the 16 Zn^{2+} form seen in 1b4e, we cannot report any significant differences in the first or second coordination spheres of the metal ion that are outside the uncertainty of the structure determination. The site is typical of an octahedral Mg^{2+} complex with oxygen ligands, five of which derive from H_2O and one from Glu-231. Octahedral, all-oxygen coordination is atypical of protein-bound Zn^{2+} . For the six ligands to the metal in the MgC site, the oxygen– Zn^{2+} bond distances of 1b4e (1.9–2.1 Å) are marginally shorter than the oxygen– Mg^{2+} distances found here (2.0–2.2 Å). The Mg^{2+} environment does not show communication with lysine residues on the active site lid as had been seen in 1b4k. Since we see no structural differences between Zn^{2+} and Mg^{2+} in this site, we propose that it is the rigidity of the Mg^{2+} that causes the allosteric effect relative to Zn^{2+} , which is far more accommodating of coordination changes (28).

In addition to the 8 Mg^{2+} which bind to the MgC site, *E. coli* PBGS has 8 Zn^{2+} , whose location and function have been subject to a variety of inadequate interpretations (e.g., refs 13 and 26). The *E. coli* PBGS structure 1b4e contains Zn^{2+} in the cysteine-rich site at high occupancy. The current structure also shows that each of the subunits contains one Zn^{2+} comparable to the ZnB of human PBGS at 100% occupancy. We herein conclude that *E. coli* PBGS does not contain a divalent metal ion binding site comparable to the 4 ZnA sites of human PBGS and that the 8 Zn^{2+} of *E. coli* PBGS are equivalent and catalytically essential. Since the ZnA site was shown to be a determinant for the high susceptibility of human PBGS to inhibition by Pb^{2+} (18), this conclusion is consistent with the observation that *E. coli* PBGS is far less susceptible to inhibition by the heavy metal toxin lead than is human PBGS.

DISCUSSION

Proposed PBGS Reaction Mechanism. The first step in the PBGS-catalyzed reaction is the binding of P-side ALA and subsequent formation of a carbinolamine intermediate between the keto group of P-side ALA and Lys-246 (numbered for *E. coli* PBGS). The carbinolamine is the precursor to the P-side Schiff base. The formation of this first Schiff base yields one water molecule formally derived from the C4 oxygen of P-side ALA and two protons from the ϵ -amino group of Lys-246. Lys-194 is positioned to act

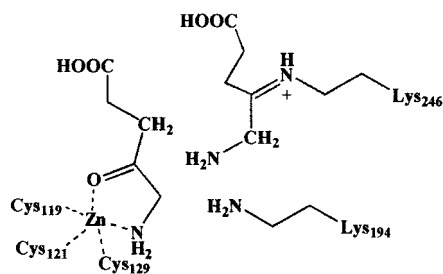


FIGURE 7: Proposed structure for the ternary complex of the Zn-utilizing PBGS with P-side ALA as the Schiff base intermediate and A-side ALA poised to form a second Schiff base to the amino group of P-side ALA or to a second active site lysine.

as a buffer for these proton-transfer reactions as has been postulated (2). The distance between the ϵ -amino group of Lys-194 and that of Lys-246 is ~ 2.7 – 4.8 Å in available PBGS structures. The stereochemistry and protonation state of the P-side Schiff base are drawn in Figure 7 according to the results of a series of ^{13}C and ^{15}N NMR studies (29). The formation of the P-side Schiff base does not require divalent metal ions (30) and appears to be common to all of the PBGS. The crystal structures of PBGS provide no solid data on the fate of the H_2O molecule that derives from P-side Schiff base formation. In fact, the P-side binding pocket is formed by a group of conserved hydrophobic residues, which in *E. coli* PBGS are Phe-78, Tyr-191, Tyr-200, Phe-203, Tyr-269, and Val-271, as can be seen in Figure 5A. This hydrophobic site could be considered hostile to a water molecule. However, there are a significant number of ordered water molecules that lie near the A-side ALA binding pocket. It is possible that the formation and translocation of the water derived from P-side ALA are part of what triggers the closing of the lid and the formation of the A-side ALA binding pocket.

The next step in the PBGS-catalyzed reaction is the binding of A-side ALA, which has been shown in mammalian PBGS to require the presence of the catalytic Zn^{2+} (30). The transient ternary complex, illustrated in Figure 7, cannot be observed because the production of porphobilinogen inevitably follows. It has been proposed that Zn^{2+} acts to polarize the C4 carbonyl of A-side ALA, and ^{13}C and ^{15}N NMR studies suggested that the free amino group of porphobilinogen is coordinated to the Zn^{2+} (29). Hence, the C4 carbonyl and the C5 amino group of A-side ALA are drawn in Figure 7 as a bidentate ligand to the catalytic Zn^{2+} , not unlike that seen in carboxypeptidase (31). However, the direct coordination between the A-side ALA amino group and the catalytic Zn^{2+} is not fully consistent with all prior inhibition studies and awaits resolution (9).

From this point in the reaction, there are three possible chemical pathways. One involves carbon–carbon bond formation between the two substrate molecules. This mechanism for *E. coli* PBGS is not supported by inhibition data (11). The other two pathways involve carbon–nitrogen bond formation, in one case between substrates and in the final case between A-side ALA and Lys-194. Because the C5 amino group of the P-side Schiff base is uncharged, carbon–nitrogen bond formation between substrates has been a favored mechanism (29). The PBGS inhibitor 4,7-DOSA is designed to mimic the di-Schiff base intermediate that would result (11). It is noteworthy that in a model of the enzyme-

bound P-side Schiff base intermediate the invariant amino group of Lys-194 is positioned only ~ 3.0 Å from the free amino group of the P-side Schiff base intermediate and could help to maintain the basic environment and favor formation of the second Schiff base (model not shown). Thus, Lys-194 may serve a dual role in facilitating the formation of both Schiff base intermediates.

One would expect that if one role of the Zn^{2+} is to polarize the C4 carbonyl of A-side ALA, then the water molecule that is the second product of the Schiff base formation reaction would end up as a ligand to the Zn^{2+} . As seen in the enzyme-bound complex with 4,7-DOSA, a water molecule is indeed present as expected. However, 4,7-DOSA does not provide the N_{11} amino group of porphobilinogen which, based on our ^{13}C and ^{15}N NMR studies, has long been proposed to act as a Zn^{2+} ligand (29). Both 4-coordinate and 5-coordinate catalytic Zn^{2+} are common. The Zn^{2+} environment supports its role in polarizing the C4 carbonyl of A-side ALA but does not address whether the resulting Schiff base forms to P-side ALA or to Lys-194.

In the normal PBGS-catalyzed reaction, two protons that formally end up as water are derived from C3 of A-side ALA (here analogous to C8 of 4,7-DOSA), and one proton derives from C5 of P-side ALA (here analogous to C5 of 4,7-DOSA). Inspection of the structure obtained herein shows the C3 protons as pointing toward two potential bases. One C3 proton appears poised to be plucked off by the Zn^{2+} -bound water or hydroxyl group. The other C3 proton is poised to interact with Lys-194. Removal of one of these protons will alter the geometry of C3 and likely render the other base ineffective. The second proton formally ends up on Lys-246. Hence, the current structure provides no more certainty as to the identity of the base that abstracts the first C3 proton than previous structures (2).

The structural results presented here suggest a third mechanistic possibility that follows formation of the ternary complex illustrated in Figure 7. In this pathway, an enzyme–substrate Schiff base is formed between the Zn^{2+} -polarized carbonyl of A-side ALA and the ϵ -amino group of Lys-194. In this case, one would call 4,7-DOSA a bisubstrate analogue rather than an intermediate analogue. In this mechanism, the two Schiff bases are almost parallel and thus perfectly situated for an aldol-type reaction during which one Schiff base is transformed into an enamine and the other one stays as an activated iminium ion.

One significant contribution of the current structure is the visualization of inhibitor atoms C6–C10 analogous to C1–C5 of A-side ALA and direct visualization of the interaction of the C10 carboxyl group with three residues from the active site lid, Arg-204, Arg-215, and Gln-219 (see Figure 6). This is a strong indication that lid closing is associated with A-side ALA binding. More significantly, however, it points to a good reason for lid mobility in the PBGS reaction mechanism. The structure shows tight binding of the propionyl side chain of P-side ALA, and we have evidence that the Zn^{2+} stabilizes the amino end of A-side ALA. During the reaction there are significant hybridization changes, particularly at C3 of A-side ALA. To accommodate these changes, we propose that the acetyl side chain experiences substantial mobility throughout the course of the reaction. In support of this notion, there are multiple hydrogen bonds between the C10 carboxyl and Arg-204, Arg-215, and Gln-219 which

might change in possible conformations. It is also interesting to note that one sees a cushion of water molecules (water bed) beside the proposed A-side ALA which can also move to accommodate the necessary hybridization changes.

CONCLUDING REMARKS

We describe here a proposed reaction intermediate analogue inhibitor 4,7-DOSA that binds irreversibly the PBGS active site, shows dramatic species-selective inhibition, and is highly effective against human PBGS. Thus, 4,7-DOSA and related compounds could be used as lead molecules in the development of highly efficient and class-selective inhibitors against human PBGS and also against various pathogens affecting humans. For example, succinyl acetone (4,6-dioxoheptanoic acid) is a physiologic byproduct of defective fumarylacetoacetate hydrolase in hereditary tyrosinemia (32) and also a commonly used inactivator of PBGS (e.g., ref 33). Although the exact mechanism is still unknown, succinyl acetone has been shown to be a potent immunosuppressive agent in the prevention of graft vs host disease after bone marrow transplantation in rats (34). In vitro succinyl acetone has also been indicated to act as a chemotherapeutic agent against some leukemias (35). The malaria-causing pathogen *Plasmodium* uses host heme biosynthetic enzymes rather than a salvage pathway to sustain heme synthesis during infection, and succinyl acetone has been shown to inactivate parasite heme biosynthesis in a concentration-dependent manner (36). Thus, PBGS could be used as a novel drug target for the treatment of malarial disease.

ACKNOWLEDGMENT

The authors acknowledge Ms. Erin Ross, whose science fair project was the initial crystallization trials of 4,7-DOSA with *E. coli* PBGS. Mr. Jacob Martins and Drs. Nicole Frankenberg, Robert Petrovich, and Laura Mitchell are acknowledged for their essential roles in purifying the various PBGS enzymes studied. Dr. Jenny P. Glusker is acknowledged for helpful discussion.

REFERENCES

- Erskine, P. T., Senior, N., Awan, S., Lambert, R., Lewis, G., Tickle, I. J., Sarwar, M., Spencer, P., Thomas, P., Warren, M. J., Shoolingin-Jordan, P. M., Wood, S. P., and Cooper, J. B. (1997) *Nat. Struct. Biol.* 4, 1025–1031.
- Erskine, P. T., Norton, E., Cooper, J. B., Lambert, R., Coker, A., Lewis, G., Spencer, P., Sarwar, M., Wood, S. P., Warren, M. J., and Shoolingin-Jordan, P. M. (1999) *Biochemistry* 38, 4266–4276.
- Frankenberg, N., Erskine, P. T., Cooper, J. B., Shoolingin-Jordan, P. M., Jahn, D., and Heinz, D. W. (1999) *J. Mol. Biol.* 289, 591–602.
- Erskine, P. T., Newbold, R., Roper, J., Coker, A., Warren, M. J., Shoolingin-Jordan, P. M., Wood, S. P., and Cooper, J. B. (1999) *Protein Sci.* 8, 1250–1256.
- Kervinen, J., Dunbrack, R. L., Jr., Litwin, S., Martins, J., Scarrow, R. C., Volin, M., Yeung, A. T., Yoon, E., and Jaffe, E. K. (2000) *Biochemistry* 39, 9018–9029.
- Boese, Q. F., Spano, A. J., Li, J. M., and Timko, M. P. (1991) *J. Biol. Chem.* 266, 17060–17066.
- Chauhan, S., Titus, D. E., and O'Brian, M. R. (1997) *J. Bacteriol.* 179, 5516–5520.
- Petrovich, R. M., Litwin, S., and Jaffe, E. K. (1996) *J. Biol. Chem.* 271, 8692–8699.
- Neier, R. (1996) *Adv. Nitrogen Heterocycl.* 2, 35–46.
- Luond, R. M., Walker, J., and Neier, R. W. (1992) *J. Org. Chem.* 57, 5005–5013.
- Jarret, C., Stauffer, F., Henz, M. E., Marty, M., Luond, R. M., Bobalova, J., Schurmann, P., and Neier, R. (2000) *Chem. Biol.* 7, 185–196.
- Jaffe, E. K., Volin, M., Bronson-Mullins, C. R., Dunbrack, R. L., Jr., Kervinen, J., Martins, J., Quinlan, J. F., Jr., Sazinsky, M. H., Steinhouse, E. M., and Yeung, A. T. (2000) *J. Biol. Chem.* 275, 2619–2626.
- Mitchell, L. W., and Jaffe, E. K. (1993) *Arch. Biochem. Biophys.* 300, 169–177.
- Frankenberg, N., Jahn, D., and Jaffe, E. K. (1999) *Biochemistry* 38, 13976–13982.
- Cheung, K. M., Spencer, P., Timko, M. P., and Shoolingin-Jordan, P. M. (1997) *Biochemistry* 36, 1148–1156.
- Jaffe, E. K. (2000) *Acta Crystallogr., Sect. D* 56, 115–128.
- Mitchell, L. W., Volin, M., Martins, J., and Jaffe, E. K. (2001) *J. Biol. Chem.* 276, 1538–1544.
- Jaffe, E. K., Martins, J., Li, J., Kervinen, J., and Dunbrack, R. L., Jr. (2001) *J. Biol. Chem.* 276, 1531–1537.
- Frankenberg, N., Heinz, D. W., and Jahn, D. (1999) *Biochemistry* 38, 13968–13975.
- Astrin, K. H., Bishop, D. F., Wetmur, J. G., Kaul, B., Davidow, B., and Desnick, R. J. (1987) *Ann. N.Y. Acad. Sci.* 514, 23–29.
- Otwinowski, Z., and Minor, W. (1997) *Methods Enzymol.* 276, 307–326.
- Navaza, J. (1994) *Acta Crystallogr., Sect. A* 50, 157–163.
- Brunger, A. T., Adams, P. D., Clore, G. M., DeLano, W. L., Gros, P., Grosse-Kunstleve, R. W., Jiang, J.-S., Kuszewski, J., Nilges, M., Pannu, N. S., Read, R. J., Rice, L. M., Simonson, T., and Warren, G. L. (1998) *Acta Crystallogr., Sect. A* 54, 905–921.
- Jones, T. A., Zou, J. Y., Cowan, S., and Kjeldgaard, M. (1991) *Acta Crystallogr., Sect. A* 47, 110–119.
- Copeland, R., Lombardo, D., Giannaras, J., and Decicco, C. (1995) *Bioorg. Med. Chem. Lett.* 5, 1947–1952.
- Spencer, P., and Jordan, P. M. (1994) *Biochem. J.* 300, 373–381.
- Jaffe, E. K., Ali, S., Mitchell, L. W., Taylor, K. M., Volin, M., and Markham, G. D. (1995) *Biochemistry* 34, 244–251.
- Glusker, J. P., Katz, A. K., and Bock, C. W. (1996) *Acta Crystallogr., Sect. A* 52, 133.
- Jaffe, E. K., Markham, G. D., and Rajagopalan, J. S. (1990) *Biochemistry* 29, 8345–8350.
- Jaffe, E. K., and Hanes, D. (1986) *J. Biol. Chem.* 261, 9348–9353.
- Christianson, D. W., and Lipscomb, W. N. (1986) *Proc. Natl. Acad. Sci. U.S.A.* 83, 7568–7572.
- Paradis, K. (1996) *Clin. Invest. Med.* 19, 311–316.
- Tschudy, D. P., Hess, R. H., and Frykholm, B. C. (1981) *J. Biol. Chem.* 256, 9915–9923.
- Fidler, J. M., Chang, T. Q., Bauer, R., Young, J. D., and Vitt, C. R. (1993) *Transplantation* 55, 367–373.
- Castaneda, V. L., Parmley, R. T., Pinnix, I. B., Raju, S. G., Guzman, G. S., and Kinkade, J. M. (1992) *Exp. Hematol.* 20, 916–924.
- Srivastava, P., and Pandey, V. C. (1998) *Exp. Parasitol.* 88, 60–63.

BI010656K